IOP Publishing Journal of Micromechanics and Microengineering
J. Micromech. Microeng. **21** (2011) 054024 (8pp) doi:10.1088/0960-1317/21/5/054024

Scaling deterministic lateral displacement arrays for high throughput and dilution-free enrichment of leukocytes

David W Inglis[1], Megan Lord[2] and Robert E Nordon[2]

[1] Department of Physics and Astronomy, Macquarie University, NSW 2109 Australia
[2] Graduate School of Biomedical Engineering, University of New South Wales, NSW 2052 Australia

E-mail: david.inglis@mq.edu.au

Received 20 January 2011, in final form 7 April 2011
Published 28 April 2011
Online at stacks.iop.org/JMM/21/054024

Abstract
A disposable device for fractionation of blood into its components that is simple to operate and provides throughput of greater than 1 mL min^{-1} is highly sought after in medical diagnostics and therapies. This paper describes a device with parallel deterministic lateral displacement devices for enrichment of leukocytes from blood. We show capture of 98% and approximately ten-fold enrichment of leukocytes in whole blood. We demonstrate scaling up through the integration of six parallel devices to achieve a flow rate of 115 μL of undiluted blood per minute per atmosphere of applied pressure.

S Online supplementary data available from stacks.iop.org/JMM/21/054024/mmedia

(Some figures in this article are in colour only in the electronic version)

1. Introduction

Fractionation of blood into its cellular components is a core technology for cellular diagnostics and transfusion medicine. Current methods employ density centrifugation and/or chemical lysis to remove red blood cells from whole blood and to enrich leukocytes (white blood cells) which are present at relatively low frequency (1:1000). Leukocyte concentrates can be sub-fractionated into platelets, lymphocytes, monocytes and granulocytes by centrifugation through a density gradient. Centrifugal methods, such as apheresis and centrifugal elutriation, require operator skill, while throughput is limited by the capacity of the centrifuge system. Red blood cell lysis is a common step in the isolation of leukocytes, though it is potentially damaging to leukocytes, and may require additional centrifugal washing steps to remove red cell debris. Ficoll centrifugation requires equipment, chemicals, skill, and typically only collects mononuclear cells. We are working toward a disposable chip that produces enriched leukocytes without chemicals or laboratory equipment.

Active separation methods such as fluorescence activated electrostatic droplet sorting (FACS) have great selectivity, but limited throughput (10 000 cells s^{-1}) because cells are separated one at a time. Passive separation methods that require antibody labels include magnetic assisted cell separation (MACS) and adhesion-based systems [1], such systems have higher costs and demanding storage requirements to preserve the antibodies. Passive separation methods that do not use labels include margination [2, 3], inertial focusing [4], passive magnetic separations [5], dielectrophoresis [6], lab-on-a-CD [7], standing acoustic waves [8] and others that use microfabricated obstacles to affect the path of cells based on their size [9–12]. Most of the label-free passive separation methods do not have the size resolution required to differentiate red blood cells from leukocytes with high efficiency, and the separation efficiency of these methods typically decreases with increasing haematocrit [9–12]. Recent work on acoustic particle and blood cell separation is very encouraging, although processing large volumes requires a high power transducer [13]. Hence, there is a need for high throughput, simple and cost-effective methods to isolate leukocytes from whole blood.

Deterministic lateral displacement (DLD) has the necessary size resolution to separate leukocytes from red blood cells, does not require a power source and, as this paper

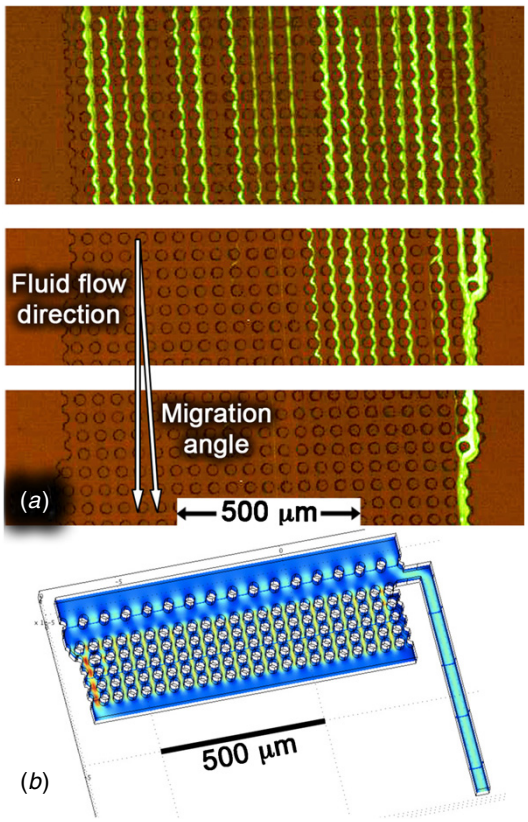

Figure 1. (*a*) Images demonstrating the concentration concept of the DLD device with fluorescent beads. The behavior is enabled by appropriate treatment of boundaries. (*b*) Results of FEM modeling of the incompressible fluid flow around the section-2 bypass. The model indicates that the flux from one gap in section 1 is drawn into the bypass when the bypass is 408 μm long for five rows of posts in section 2.

demonstrates, is able to enrich components of undiluted blood. DLD is a microfluidic particle separation method that takes advantage of the laminar nature of low Reynolds number fluid flow around obstacles. The method is passive as the cells simply flow through the device and size-separated cells are collected at specific outputs. Separation performance is not dependent on flow speed and operates as a simple filter.

A DLD device operates according to the following principle. Obstacles in fluid are positioned to cause repeated lateral displacement of particles (figure 1(*a*)). The displacement experienced by a particle depends on its hydrodynamic radius and the array geometry; particles below a critical size pass through the array of obstacles unaffected, while particles above the critical size move laterally at a pre-set angle θ.

The array of obstacles is typically a square array of circular posts that have been tilted relative to the flow. The critical size is principally affected by the tilt angle of the array (θ), or row shift fraction, and the gap between the posts, G. For arrays where $1/(\tan(\theta))$ is an integer, N, fluid flowing through the gap can be viewed as N identical, periodic streamlines, where the first and second streamlines are bifurcated by a post in the next row. If a particle is small enough to fit in the first streamline, it will follow the fluid flow direction. If a particle does not fit in the first streamline, it will be 'bumped' into the second streamline at every post and follow the angle θ, hence the colloquial term of 'bump array.'

Most earlier work has used this method to separate particles. This device concentrates particles by forcing them against one wall as shown in figure 1(*a*). This idea was demonstrated by Huang *et al* in 2004 [14], but recent work dealing with the edges of the arrays [15] has made it possible to deterministically concentrate particles into a single, edge-adjacent gap. Both edges of the array used in this study have been corrected accordingly for improved performance.

The aim of this study is to develop a passive, high throughput, disposable device for direct collection of leukocytes from whole blood, without any pre- or post-conditioning. In contrast to previous work that has used two inputs, a blood and a buffer input [16–18], we use a single input only. A single input simplifies blood separation and facilitates concentration of leukocytes with reduced separation times, which are important considerations for clinical use. Furthermore, this work demonstrates integration in a full polymer device capable of being moulded, achieving high volume throughput at minimal device cost.

2. Experimental details

2.1. Device design

A prototype device was designed to concentrate leukocytes from whole blood and to establish a proof of principle for scale-up of this device using parallel DLD devices. The design considerations for separation of leukocytes from red blood cells and integration of parallel devices are described in detail below.

2.1.1. Particle size range. The primary consideration for device design is the requirement to bump the leukocytes and avoid clogging in the array. Previous work has shown that an array with a critical size between 4 and 5 μm will bump at least 99.9% of leukocytes [16, 17]. Leukocytes larger than 20 μm are extremely rare, though cell aggregates and clots in excess of 20 μm can be common. Structures upstream of the array help to catch these before they reach the array. Hence, this device is designed to bump cells ranging in size from 4.5 to 22 μm, which is a wider range than is typically handled in a single array. From Inglis *et al* [19], we can estimate the critical size for various arrays. A slope, row shift fraction, or epsilon, ε of $1/20 = 0.05$ gives a critical size that is roughly one third of the gap. A $1/20$ array has a bump angle of $\tan^{-1}(1/20) = 2.86^\circ$, and repeats itself every 20 rows. The 22 μm gap that we have chosen above could then bump cells larger than $22/3 = 7.3$ μm, which is not small enough to collect all the leukocytes. A slope, or ε of $1/50$ should give a critical size that is close to 0.2 times the gap, $22 \times 0.2 = 4.4$ μm. However, there are very little data at this very low epsilon, and a $1/50$ array is more than twice as long as two $1/20$ arrays, so we have not used the $1/50$ array.

Table 1. Array parameters.

Section	ε	Post (μm)	Gap (μm)	Pitch (μm)	Width (μm)	Columns	Length (μm)
§1	0.05	22	22	44	836	19	26 367
§2	0.05	22	13	35	840	24	25 868

Our design uses two arrays in series, each with a slope, ε, of 1/20. Section 1 has a gap of 22 μm which is expected to move cells in the range of 7.3–22 μm. Section 2 must have a critical size of around 4.5 μm, so a gap of 13 μm (3 × 4.3 μm) was chosen. This design must include a separate pathway, or bypass, to carry the 13–22 μm cells that would otherwise clog section 2. These cells are taken to a dedicated 'large' particle exit. Cells separated by section 2 are taken to a 'medium' particle exit, while the remaining cells are taken to a 'small' particle exit. In a clinical device, the large and medium outputs would likely flow to a single output, but for our investigative purposes it is better to separate them to demonstrate the enrichment efficiency of this device.

2.1.2. Post-height and diameter. Tall posts lead to a higher throughput, but the post aspect ratio is limited by the molding step. Polydimethylsiloxane (PDMS) posts with an aspect ratio that is more than 2 have an unacceptably high probability of tipping over during assembly. An aspect ratio of 2 for an injection molded plastic device is at the limit of current manufacturing methods. As this device is meant to examine feasibility of scale-up using mass production methods this aspect ratio was chosen. Increasing post-diameter at a fixed aspect ratio may increase the throughput, but it does increase the total device area. Extremely large posts, relative to the gap also reduce the critical size, whereas extremely small posts are expected to increase the shear rate. We choose posts that are of the same size as the largest gap, 22 μm, with a depth of 40 μm.

2.1.3. Substrate size. Our substrate is a standard microscope slide (25 × 75 mm). The separation array is 52.2 mm long which allows a 5 mm boarder as well as 13 mm space at the top and bottom for inputs and outputs. We have used arrays that are 1.4 times longer than is ideally necessary to bump all the target cells, accounting for possible defects in the array. The array parameters are given in table 1.

2.1.4. Collecting the small, medium and large fractions. Sections 1 and 2 are designed to concentrate target cells into a single gap at the array edge. Section 1 has 19 columns, so the bypass channel that carries large cells around section 2 must draw 1/19th of the total flow (figure 1(*b*)). This is achieved by balancing the resistances of downstream paths. At the end of section 2, which has 24 columns, leukocytes above a particular size will flow in a single column adjacent to the wall where they can be collected. This means drawing 1/24th of the total fluid flux from section 2. Ideally, then 1/19 = 5.3% of fluid goes to the large output, 18/(19 × 24) = 3.9% goes to the medium output and the rest, 90.8% goes to the small output. This gives a theoretical maximum particle enrichment of 19 in the large output and 24 in the medium output.

A combination of modeling using COMSOL Multiphysics and analytical calculations of fluid resistance for rectangular channels was used to determine the lengths and widths of the channels that collect fluid and particles from the arrays. Equation (1) gives the resistance per meter of a rectangular channel in units of Pa/m per m^3. The relationship is obtained through an integration of velocity in a square channel, $u(x, y)$ in Brody *et al* 1996 [20]. For comparing combinations of rectangular tubes, this equation is evaluated using a spreadsheet:

$$R = \frac{\eta\pi^4}{8w^3d} \times \frac{1}{\sum_{L=0}^{\infty} \frac{1}{(2L+1)^4} - \frac{2w\ \sinh(\frac{\pi d(2L+1)}{2w})}{\pi d(2L+1)^5 \cosh(\frac{\pi d(2L+1)}{2w})}}. \quad (1)$$

In cases where the resistance of the array, as opposed to a simple tube, must be known precisely, the analytical method is not adequate. FEM models were created to simulate the entrances to the 'small' and 'medium' channels. Adjustments to the lengths of the exit channels were made until they carried the correct volume fraction. Figure 1(*b*) shows one such model. Our analytical and numerical calculations neglect shear- and density-dependent viscosity that may arise with blood [21]. Experiments with fluorescent beads in water show close to ideal volume flow branching, and volume fractions obtained with blood are close to ideal.

2.1.5. Parallel device integration. A single long and narrow device makes poor use of a substrate area and has poor volume throughput. Placing many in parallel increases the volume throughput, but necessitates three levels of fluidics to combine the outputs of parallel devices together into a single output. As a proof of concept, this device has six parallel devices. Mirroring the devices into three pairs reduces the number of vertical fluid interconnects, vias, to 8. These vias are the second level which carry fluid to level 3 which must also be matched with resistance. Figure 2 shows the layout of the device. Table 2 shows the dimensions and calculation of resistance in level 3 channels (green in figure 2). The calculated hold-up volume of the device is 16.7 μL. This approach can be applied to a device with many more than six parallel devices.

2.2. Mold fabrication

Layouts were designed using L-Edit (Tanner EDA, USA), and photolithography masks were created by the Bandwidth Foundry (Australia). The 40 μm high level 1 was made by standard SU-8 (Gersteltech, Switzerland) lithography using a 360 nm long-pass filter on a 3″ silicon wafer, wafer 1 in figure 3. Two devices were fabricated on each wafer. After hard baking, the second level containing vertical interconnects was created on top of level 1 on wafer 1. These posts are 150 μm tall (from wafer level). Rapid development is critical to prevent swelling of level 1 features. Level 3, also 150 μm high, was patterned on a 4″ wafer, wafer 2, by similar SU-8 lithography.

Table 2. Resistance calculations for level 3 fluidics.

	Length (μm)	Width (μm)	Depth (μm)	Resistance/m $\times$ 10^{13} (Ns mm^{-6})	Fluid Flux (AU)	Pressure Drop $\times$ 10^{16} (AU)
Small left	5747	316	150	1.60	2 $\times$ 0.908	16.7
Small middle	6900	361	150	1.33	2 $\times$ 0.908	16.7
Small right	7917	400	150	1.16	2 $\times$ 0.908	16.7
Medium	12 500	150	150	5.61	6 $\times$ 0.039	16.6
Large upper	8500	150	150	5.33	6 $\times$ 0.053	14.3
Large lower	6900	154	150	5.61	2 $\times$ 0.053	4.1

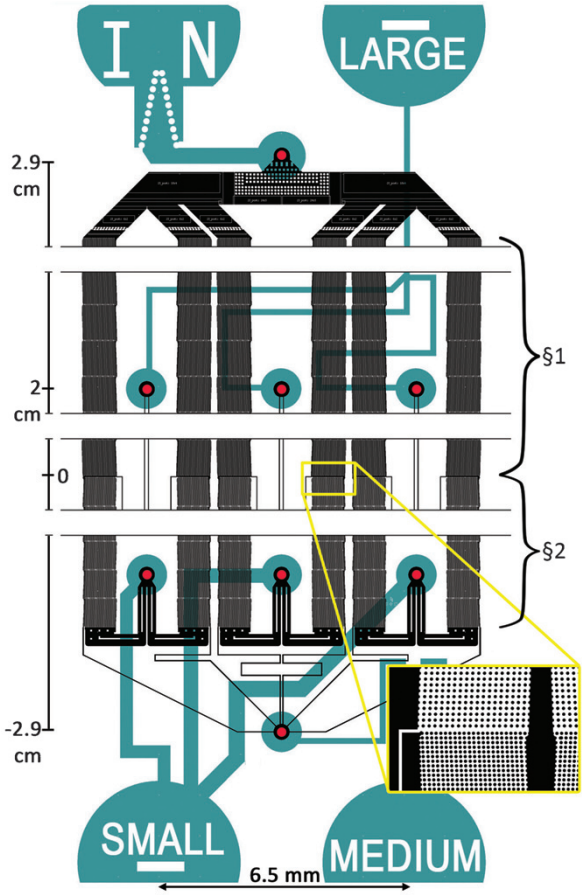

Figure 2. Device layout where level 1 is black, level 2 is red and level 3 is green. Flow is from the top port labeled 'IN' with the majority of flow going out to the lower left port labeled 'SMALL'.

2.3. Device construction

The layer 1 wafer was spin coated with freshly mixed PDMS (RTV-615 Momentive USA) at 800 rpm for 60 s, then allowed to rest for 30 min, before curing for 2 h in a 75 °C oven (figure 3). Layer 3 was formed by casting a thick, 1–2 mm, layer of degassed PDMS on the layer 3 wafer. After mould separation, holes for input and outputs were cut into this layer using a modified 19-gauge syringe needle. Layer 3 and the PDMS-coated layer 1 wafer were exposed to an oxygen plasma, then aligned and bonded using an MJB3 mask aligner (Karl Suss).

The multilayer device was then released from the wafer and vias were inspected. About 25% of the vias were manually opened by lancing with a fine gauge needle. This piece was then bonded to a PDMS-coated glass slide using the same oxygen plasma method (figure 3). Light pressure was needed in places to create complete contact. Finally, short sections of silicone tubing were pushed into the input and 'small' output and glued in place with PDMS. 'Medium' and 'large' output ports which produce only 40–50 μL for every mL of input were widened and left as reservoirs.

After this final curing step, the device was inspected then immersed in water containing 2 g L^{-1} of a block co-polymer surfactant, F108. The immersed device was placed in a bell jar which was evacuated for at least 2 h. Upon removal from the bath the device was bubble free and ready to use. Figure 4 shows scanning electron microscope images and a photograph of the device.

2.4. Operating the device

Prior to operating with beads, the device was flushed with de-ionized water containing 0.1% (v/v) Tween-20 (Sigma Aldrich, Australia) for 5 min. The mixture of beads at a total density of approximately 0.002% solid was connected and run for 20 min. The output fractions were collected and analyzed by flow cytometery (BD FACSort™). 1.9 μm diameter beads, which are not affected by the separation array, were used to calculate changes in concentration of larger beads with diameters of 5.7, 7.3 and 10 μm.

Prior to operating with blood, the device was flushed with the AutoMACS buffer (Miltenyi Biotech, Australia), a phosphate buffered saline containing EDTA and bovine serum albumin for 5 min. Whole blood or blood diluted with this buffer was then connected and run for 20 min. Total volume throughput in this time ranged from 300 to 1200 μL. The medium and large fractions were manually collected from the reservoirs. The small output was collected in a 2.5 mL flow cytometry vial by a short silicone tube. The volume in each fraction was recorded. Devices were used for two runs then discarded.

Recent work has demonstrated that PDMS devices deform considerably under pressure [22]. In order to avoid pressure-induced changes in the gaps, and consequently the critical sizes, devices were operated at 3.0 psi (0.2 atm) only. Data are presented per atm (1 atm = 14.7 psi).

2.5. Analysis of blood

Seven runs were analyzed in a Vi-Cell automated cell viability analyzer (Beckman Coulter, Australia) which measured the

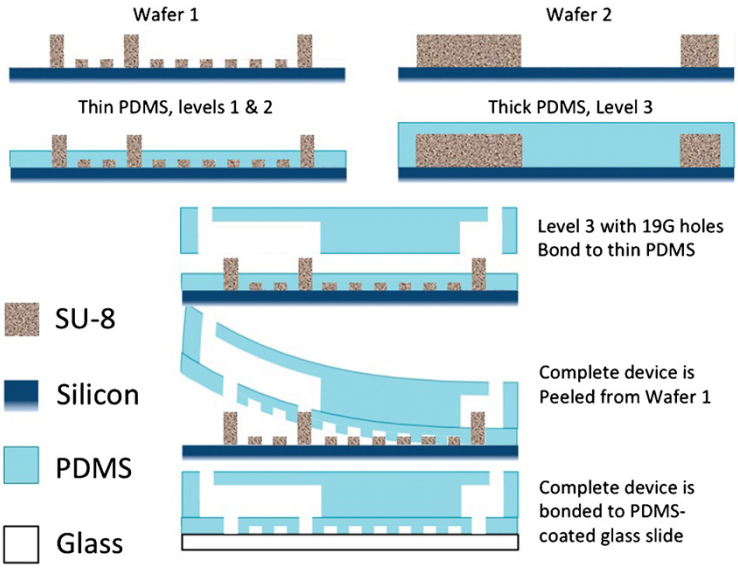

Figure 3. Illustration of fabrication steps. Wafers 1 and 2 are created by standard SU-8 photolithography. Wafer 1 is coated with a thin (50–100 μm) layer of PDMS, while wafer 2 is coated with a thick layer. The PDMS layers are aligned and bonded before peeling and assembling the final device.

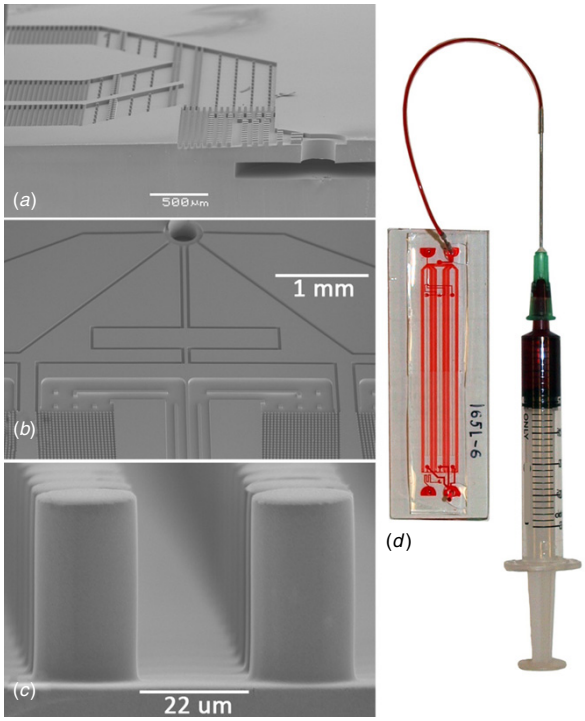

Figure 4. Various views of the device. (*a*) All three layers of the device: level 1 on top, the level 2 via at the INPUT, and the buried level 3. (*b*) Level 1 features at the downstream end the device. (*c*) Posts in section 1, note the vertical walls and small gap-width variation. (*d*) A photograph of the device containing a food dye solution connected to a 3 mL syringe.

number of cells per mL as well as the size of the cells through image cytometry. Red blood cells were lysed and remaining cells fixed using the BD FACS lysing solution prior to analysis. Another ten experiments were analyzed using a flow cytometer with BD Trucount tubes. These samples were labeled with Syto 11 (Invitrogen, Australia) to allow gating of nucleated cells, then lysed with the BD FACS lysing solution. This gives the concentration of nucleated cells with the ability to identify lymphocytes, monocytes and granulocytes based on forward and side scatter profiles. The concentration of cells in the various fractions can then be compared with the concentration in the input blood.

Blood was harvested from human donors under ethics approval in buffered sodium citrate treated vacutainers (BD Australia) and used for experimentation within 36 h of collection.

3. Experimental results and discussion

3.1. Results

The average volume flow rate for whole undiluted blood (hematocrit between 0.41 and 0.45) was 115 μL min^{-1} atm^{-1}. The flow rates for each run are shown in figure 5. The cellular flow rate, or cell-sorting rate, is the total number of cells, including red blood cells, flowing through the device per second per atmosphere of pressure applied. The cellular flow rate for each run is shown in figure 5(*b*), while the average flow rate when using undiluted blood is 9.6 million cells s^{-1} atm^{-1}. Hematocrit correlated negatively with the volume flow rate and positively with the cellular flow rate shown in figures 5(*a*) and (*b*). The volume flow rate decreased if anticoagulated blood was separated after 24 h of storage at room temperature.

Volumetric flow to each output was very close to the design expectations. The small output received 91% $\pm$ 1%,

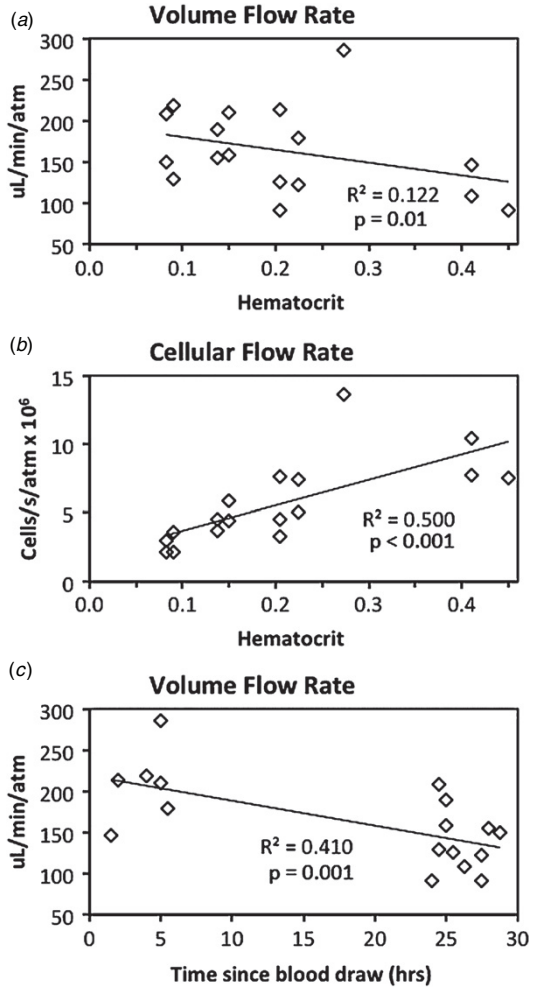

Figure 5. (*a*) Volume flow rate versus hematocrit. (*b*) Cellular flow rate versus hematocrit, dominated by red blood cells. (*c*) Volume flow rate versus time since blood draw.

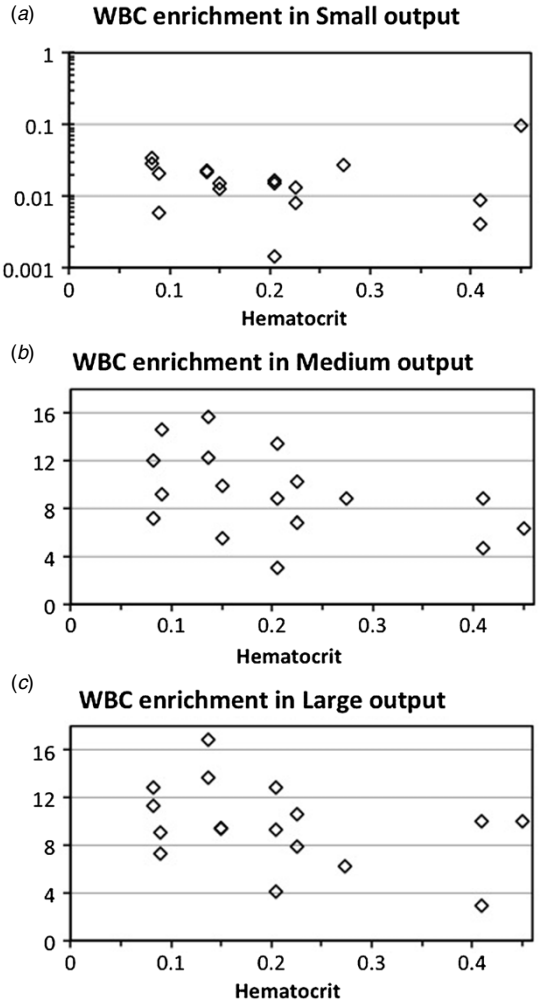

Figure 6. Leukocyte depletion and enrichment in each of the outlet streams.

the medium output received 4% ± 1%, and the large output received 5.1% ± 0.6% of the output volume. In our design, the output volume distribution was 90.8%, 3.9% and 5.3% for the small, medium and large outputs respectively; hence, the device behaved as expected. Hematocrit was not observed to effect the distribution of flow to these outputs.

Figure 6 shows changes in white blood cell concentration in the various outputs. Enrichment is defined as the output concentration divided by the input concentration, enrichment of less than 1 can be called depletion. In all but one case, leukocytes were significantly depleted in the small output compared to the input stream. Excluding this outlier, 98.7% of leukocytes were removed (1.9 log depletion). The average enrichment in the medium output was 8.6-fold, and the average enrichment in the large output was 8.9. While the output volume fractions were measured, the volume of blood entering the device was not measured.

The ability of the device to concentrate different sized particles was analyzed using beads with diameters of 5.7, 7.3 and 10 μm (figure 7(*a*)). The 10 μm beads were, in an average of six runs, enriched 17.9-fold in the medium and 4.8-fold in the large output, with 98% removal from the small output. The same effect was observed for the 7.3 μm beads, although the effect was less pronounced. The 5.7 μm beads were enriched 2.8-fold in the medium output, but scarcely altered in the other outputs streams.

The ability of the device to separate lymphocytes, granulocytes and monocytes was also analyzed (figure 7(*b*)). Monocytes and granulocytes were predominantly enriched in the large output and to a lesser extent in the medium output. Lymphocytes being the smallest of the cells analyzed are most likely to escape separation, but they were effectively sorted by the second array and were found to be enriched in the medium output by 11.8-fold. The larger monocytes were enriched by 13-fold in the large output. Vi-Cell analysis indicated that the average size of cells in the medium and large outputs were 9.3 and 10.6 μm respectively.

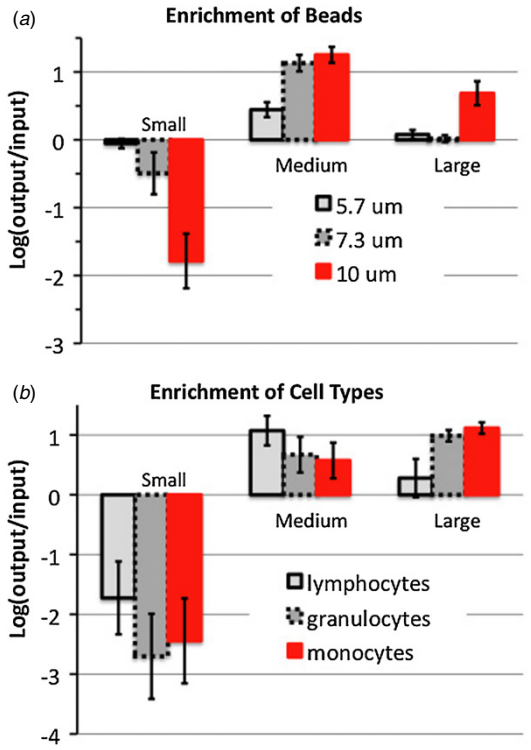

Figure 7. Plots demonstrating size selectivity of the device for (*a*) 5.7, 7.3 and 10 μm beads and (*b*) lymphocytes, granulocytes and monocytes. 10 μm beads are enriched in the medium and large outlets, while the 5.7 μm beads are weakly affected. Lymphocytes being the smallest are most likely to evade the sorting arrays, while monocytes being the largest are strongly enriched in the large output.

3.2. Discussion

We have demonstrated a path toward higher volume throughput leukocyte enrichment through parallel integration of DLD devices and careful use of the substrate real estate. We have shown processing of 9.5 million cells s^{-1} atm^{-1} in undiluted blood. The device has not achieved mL per minute throughput of whole blood for two reasons: (1) the PDMS construction and its elasticity limit the maximum applied fluid pressure and (2) only six parallel devices were used as a proof of the principle device. In future work, we plan to investigate operation at pressures up to 30 psi (2 atm), a pressure that can be achieved with the manual operation of a 5 mL syringe. A volume flow rate of approximately 200 μL min^{-1} may be achieved through operation at higher pressures and the use of more rigid plastics, as long as separation performance is not adversely affected by the increased speed and shear rate. Achieving 1 mL min^{-1} would then require 30 parallel devices. It will be possible to fit 30 arrays on a single 25 mm glass slide with minor changes in layout, including moving and shrinking vertical vias. Hold-up volume would increase accordingly, but would remain at less than 10% of the volume processed per minute.

A limit to applied pressure is imposed by shear stress. Shear can lyse red blood cells and activate platelets. Based on the volume flow rate, hold-up volume and path length, we estimate an average speed of approximately 12 mm s^{-1} at a pressure drop of 1 atm. In a 13 μm gap, the shear will be around 3000 s^{-1}, or 600 s^{-1} at the 3 psi used here. Normal blood flow experiences shear rates of up to 2000 s^{-1} [23–25]. Hence, at two atmospheres then the shear rate would clearly be higher than physiological levels, but the literature has widely varying estimates for when shear induced lysis and platelet activation occurs. Holme *et al* [24] reported shear-induced platelet activation at 10 500 s^{-1}, while Markou *et al* [25] reported no activation at shear levels up to 280 000 s^{-1}, but did see cell lysis beyond this. Increasing throughput by placing 30 devices in parallel will not change the shear rate. Further work is needed to determine what effect the shear will have on the cells and on enrichment performance.

The cell-sorting rate increases linearly with hematocrit without a significant effect on the enrichment factor. However, there was less than expected enrichment of leukocytes compared to beads. We hypothesize that leukocyte enrichment performance was limited by cell clumping which can lead to a lower leukocyte enrichment rate and device flow rate. Analysis of variance shows that the time between blood draw and experiment as well as the donor identity is a significant covariate (see ANOVA table in the supplementary online information, available at stacks.iop.org/JMM/21/054024/mmedia). The device flow rate was significantly lower if blood was separated after 24 h of storage (figure 5(*c*)). Donor variations may arise because of the large variation in the platelet count in the general population (150–400 $\times$ 10^9 L^{-1}) [26], which may influence the level of clumping inside the device even when using anticoagulated blood.

Blockages arising from large (20–200 μm) clot-like structures present in the blood were observed regularly. Most of these were filtered before the start of the enrichment array; however, blockages in these filter regions increase fluidic resistance and decrease the throughput. Cell clumps that dislodge and enter the enrichment array can alter the flow patterns and decrease the enrichment performance.

Finally, we believe that device-manufacturing flaws impact both enrichment performance and reproducibility. Due to the need to manually clear level 2 vias, the degree of clearing may be inconsistent. If an input via is not completely cleared the flow rate will be reduced, and if one of the seven output vias is not identical to the others, the flow balance to the output is altered leading to reduced enrichment performance. However, as most devices were not re-used, ANOVA did not show a significant effect of device identity on separation performance.

The device does not separate small particles as well as intended. The bump arrays were designed for the separation of particles between 4.5 and 7.3 μm; yet analysis of different sized beads indicates that 5.7 μm particles were not strongly affected. Observations of microspheres in the device show that particles just above the critical size concentrate on two, rather than one column, indicating that the edge correction strategy described in [15] is not ideal. The strategy attempts to create bulk-like flow patterns from wall to wall. An aberration to the improved array of fluid bifurcations arises where two columns of fluid merge into a single gap with width $\sqrt{2}$ times

the nominal gap. The finite post size requires that the wall adjacent column takes a longer path length than the column that is second from the wall. This perturbs the flow in adjacent gaps and locally increases the critical size. Correcting this would ensure maximum concentration and complete collection of smaller leukocytes, but we have yet to find a better solution. It is also possible to decrease the gap size, or lower the row shift fraction, though these come at the cost of reduced volume throughput.

Leukocyte enrichment generally fell short of the maximum possible factor of 19 in the large output and 24 in the medium output. This suggests that some cells are not bumped all the way to the edge adjacent column either because of downstream blockages, imperfect array design or imperfect fabrication. Cellular clumps resulting from incomplete anticoagulation and/or blood cell activation remain a significant factor limiting the performance of bump arrays. Future work will address strategies to prevent cell clumping and to optimize surface chemistry and pre-filter designs to minimize device blockages.

In conclusion, we have presented a passive, disposable, low-cost device for leukocyte concentration and collection, demonstrating the potential for mL min^{-1} processing of whole blood. Volume throughput, performance and cost are the most significant determinants for clinical application of this technology. The development of a mL min^{-1} device for point-of-care diagnostic applications is feasible by production in rigid plastic and further integration of the device presented here.

Acknowledgments

This project was principally funded by the Australian Research Council, with additional support from the Fluorescence Applications in Biology and Life Science Network. Institutional support has come from the MQ Photonics Research Center, The Physics and Engineering Clean Room at Macquarie University and the PC2 Facility at the Graduate School of Biomedical Engineering, UNSW. Photomasks were made at the Optofab node of the Australian National Fabrication Facility, established under the National Collaborative Research Infrastructure Strategy. DI thanks Graham Vesey, George Miklos and Ewa M Goldys for consistent guidance, support, and feedback.

References

[1] Wank K, Cometti B and Pappas D 2007 Isolation and counting of multiple cell types using an affinity separation *Anal. Chim. Acta* **601** 1–9

[2] Goldsmith H L and Spain S 1984 Margination of leukocytes in blood flow through small tubes *Microvasc. Res.* **27** 204

[3] Hou H W *et al* 2010 Deformability based cell margination—A simple microfluidic design for malaria-infected erythrocyte separation *Lab Chip* **10** 2605–13

[4] Mach A J and Di Carlo D 2010 Continuous scalable blood filtration device using inertial microfluidics *Biotech. Bioeng.* **107** 302–11

[5] Han K H and Frazier A B 2006 Paramagnetic capture mode magnetophoretic microseparator for high efficiency blood cell separations *Lab Chip* **6** 265–73

[6] Pommer M S *et al* 2008 Dielectrophoretic separation of platelets from diluted whole blood in microfluidic channels *Electrophoresis* **29** 1213–8

[7] Zhang J, Guo Q, Liu M and Yang J 2008 A lab-on-CD prototype for high-speed blood separation *J. Micromech. Microeng.* **18** 125025

[8] Shi J *et al* 2009 Continuous particle separation in a microfluidic channel *via* standing surface acoustic waves (SSAW) *Lab Chip* **9** 3354–3359

[9] Zheng S, Liu J Q and Tai Y C 2008 Streamline-based microfluidic devices for erythrocytes and leukocytes separation *J. Micromech. Syst.* **17** 1029–38

[10] Choi S *et al* 2007 Continuous blood cell separation by hydrophoretic filtration *Lab Chip* **7** 1532–8

[11] Chen A, Cui D F, Liu C C and Li Hui 2008 Microfluidic chip for blood cell separation and collection based on crossflow filtration *Sensors Actuators* B **130** 216–21

[12] Jäggi D, Sandoz R and Effenhauser C S 2007 Microfluidic depletion of red blood cells from whole blood in high-aspect-ratio microchannels *Microfluid. Nanofluid.* **3** 47–53

[13] Adams J D and Soh H T 2010 Tunable acoustophoretic band-pass particle sorter *Appl. Phys. Lett.* **97** 064103

[14] Huang L R, Cox E C, Austin R H and Sturm J C 2004 Continuous particle separation through deterministic lateral displacement *Science* **304** 987–90

[15] Inglis D W 2009 Efficient microfluidic particle separation arrays *Appl. Phys. Lett.* **94** 013510

[16] Davis J A, Inglis D W, Morton K J, Lawrence D A, Huang L R, Chou S Y, Sturm J C and Austin R H 2006 Deterministic hydrodynamics: taking blood apart *PNAS* **103** 14779–84

[17] Huang R *et al* 2008 A microfluidics approach for the isolation of nucleated red blood cells (NRBCs) from the peripheral blood of pregnant women *Prenat. Diagn.* **28** 892–9

[18] Inglis D W, Davis J A, Zieziulewicz T J, Lawrence D A, Austin R H and Sturm J C 2008 Determining blood cell size using microfluidic hydrodynamics *J. Immunol. Methods* **329** 151–6

[19] Inglis D W, Davis J A, Austin R H and Sturm J C 2006 Critical particle size for fractionation by deterministic lateral displacement *Lab Chip* **6** 655–8

[20] Brody J P, Yager P, Goldstein R E and Austin R H 1996 Biotechnology at low Reynolds numbers *Biophys. J.* **71** 3430–41

[21] Reinke W, Johnson P C and Gaehtgens P 1986 Effect of shear rate variation on apparent viscosity of human blood in tubes of 29 to 94 microns diameter *Circ. Res.* **59** 124–32

[22] Inglis D W 2010 A method for reducing pressure-induced deformation in silicone microfluidics *Biomicrofluidics* **4** 026504

[23] Freitas R A Jr 1999 *Nanomedicine: Basic Capabilities* vol 1 (Georgetown, TX: Landes Bioscience)

[24] Holme P, Orvim U, Hamers M J, Solum N O, Brosstad F R, Barstad R M and Sakariassen K S 1997 Shear-induced platelet activation and platelet microparticle formation at blood flow conditions as in arteries with a severe stenosis *Arterioscler. Thromb. Vasc. Biol.* **17** 646–53

[25] Markou C P, Marzec U M, Chinn J A, Hirt F and Hanson S R 1999 Shear induced platelet activation *Proc. 1st Joint BMES/EMBS Conf., Serving Humanity, Advancing Technology (Atlanta GA, USA)* p 770

[26] Lewis S M, Bain B J and Bates I 2001 *Dacie and Lewis Practical Haematology* (London: Churchill Livingstone)